

# FAT: An In-Memory Accelerator with Fast Addition for Ternary Weight Neural Networks

Shien Zhu\*, Luan H.K. Duong\*, Hui Chen\*, Di Liu<sup>†</sup>, Weichen Liu\*

\*School of Computer Science and Engineering, Nanyang Technological University, Singapore

<sup>†</sup>HP-NTU Digital Manufacturing Corporate Lab, Nanyang Technological University, Singapore

Email: shien001@e.ntu.edu.sg, {lhkduong, hui.chen, liu.di, liu}@ntu.edu.sg

**Abstract**—Convolutional Neural Networks (CNNs) demonstrate great performance in various applications but have high computational complexity. Quantization is applied to reduce the latency and storage cost of CNNs. Among the quantization methods, Binary and Ternary Weight Networks (BWNs and TWNs) have a unique advantage over 8-bit and 4-bit quantization. They replace the multiplication operations in CNNs with additions, which are favoured on In-Memory-Computing (IMC) devices. IMC acceleration for BWNs has been widely studied. However, though TWNs have higher accuracy and better sparsity, IMC acceleration for TWNs has limited research. TWNs on existing IMC devices are inefficient because the sparsity is not well utilized, and the addition operation is not efficient.

In this paper, we propose FAT as a novel IMC accelerator for TWNs. First, we propose a Sparse Addition Control Unit, which utilizes the sparsity of TWNs to skip the null operations on zero weights. Second, we propose a fast addition scheme based on the memory Sense Amplifier to avoid the time overhead of both carry propagation and writing back the carry to the memory cells. Third, we further propose a Combined-Stationary data mapping to reduce the data movement of both activations and weights and increase the parallelism of memory columns. Simulation results show that for addition operations at the Sense Amplifier level, FAT achieves  $2.00\times$  speedup,  $1.22\times$  power efficiency and  $1.22\times$  area efficiency compared with State-Of-The-Art IMC accelerator ParaPIM. FAT achieves  $10.02\times$  speedup and  $12.19\times$  energy efficiency compared with ParaPIM on networks with 80% sparsity.

## I. INTRODUCTION

Deep Convolutional Neural Networks (CNNs) have been widely adopted in computer vision [1], [2], natural language processing [3], [4], robotics [5], [6] and many other fields. Deep CNNs have numerous parameters, and the convolution layers are both memory-intensive and computation-intensive, resulting in high storage cost and long latency when deployed on the edge. So deep CNNs need optimization and acceleration for the edge to achieve low storage overhead and high performance.

Quantization is one of the effective CNN acceleration methods that reduce CNNs' computation complexity and storage cost. Quantization methods utilize low bitwidth numbers to represent the values of CNNs. Among the quantization methods, Binary Weight Networks (BWNs) [7], [8], [9] can achieve extreme storage saving and high performance thanks to their 1-bit representation of weights. BWNs quantize the weights of CNNs into  $\{+1, -1\}$  to replace the computation-intensive multiplication operations with addition and subtraction operations for high speedup, but this aggressive quantization also

TABLE I  
TOP-1 ACCURACY ON IMAGENET OF QUANTIZED RESNET-18.

Method	Type	Bitwidth	Operations	Accuracy	Sparsity
Original[20]	FP	32-bit	$\times, +$	70.3%	10-40%
U-INT8[10]	INT8	8-bit	$\times, +$	69.7%	-
ULP-INT4[13]	INT4	4-bit	$\times, +$	69.0%	-
RTN[15]	TWN	2-bit	$+$	68.5%	40-90%
LS-BQNN[9]	BWN	1-bit	$+$	66.1%	0%

leads to lower accuracy. As both the accuracy and the speed of CNNs matter, other quantization methods, including 8-bit [10], [11] and 4-bit [12], [13] integer quantization (INT8 and INT4) and ternary quantization [14], [15], [16], are proposed to do a trade-off between the speed and accuracy as Table. I shows.

Ternary Weight Networks (TWNs) [14], [15] make an excellent trade-off between BWNs and 32-bit Full-Precision (FP) CNNs. TWNs quantize the weights of CNNs into  $\{+1, 0, -1\}$  and brings several advantages, as shown in Table. I. First, TWNs have much higher accuracy than BWNs due to their higher representation capacity of weights. Second, the 2-bit representation of TWNs brings  $16\times$  storage-saving compared with the 32-bit FP CNNs. Third, the addition operation has been the dominant operation in TWNs just like BWNs, which guarantees TWNs high performance. While 8-bit/4-bit integer quantization still uses computation-intensive multiplications in the convolution layers. Last, TWNs have zeros in the weights referred to as sparsity. This means the addition operations related to zero weights can be skipped to achieve even higher performance than BWNs. The support from the hardware and programming library is essential to skipping the null operations [17], [18], [19]. Therefore, a hardware accelerator with fast and sparse addition is necessary to obtain the mentioned benefits of TWNs.

In-Memory-Computing (IMC) [21] is an excellent choice in accelerating addition-centric CNNs, including BWNs and TWNs. As deep CNNs are both memory-intensive and computation-intensive, the memory access on hardware is an essential factor in CNN performance besides the computation. Unfortunately, traditional von Neumann architecture separates the memory from the processing unit, which results in limited memory bandwidth, long memory access latency and high energy costs in transferring data between the memory and processing units. These challenges are known as the memory wall. IMC is a promising way to relieve the memory wall, uti-

lizing resistant memories like Spin-Transfer Torque Magnetic Random-Access-Memory (STT-MRAM) to compute inside the memory [22]. Thanks to the massive data parallelism, ultra-high internal memory bandwidth, and reduced data movement, IMC brings high performance and energy efficiency. In addition, state-Of-The-Art (SOTA) IMC devices can conduct Boolean functions and addition operations, making them very suitable for accelerating addition-centric CNNs [23], [24], including BWNs and TWNs.

However, though TWNs have higher accuracy and better sparsity than BWNs, current IMC accelerators have not been optimized to fit the characteristics of TWNs. First, the sparsity of TWNs is not well utilized. The sparse weights of TWNs bring the need for compressed sparse formats to save storage [25], [26]. But the compression and decompression modules of the compressed sparse format will increase the complexity of the accelerator design, the area cost and the power. It is a challenge to deal with the sparsity and the sparse data format. As a result, the sparsity of TWNs has not been exploited to skip the operations of neural networks on existing IMC accelerators. For example, TiM-DNN [27] and XNOR-SRAM [28] all process the ternary neural networks without considering the sparsity.

Also, addition operations have replaced the multiplications for higher performance in TWNs, but the addition operations in existing IMC devices are not efficient. The mainstream STT-CiM series [29], [30], [31], ParaPIM series [32], [33] and GraphS series [34], [35], [36] devices are excellent IMC designs in general-purpose and application-specific domains, but their addition schemes are not efficient. They either need to wait for the carry propagating to the last bit or write back the carry to the memory cells and read out the carry back and forth. Applying the same addition schemes directly to processing TWNs will lead to long latency and high power consumption.

In this paper, we proposed FAT as an STT-MRAM based IMC accelerator for high performance and energy-efficient TWN inference. First, we propose a Sparse Addition Control Unit at the architecture level which utilizes the sparsity of TWNs to speedup the convolution and fully connected layers. We combine the weights with the control signals of the memory arrays to skip the addition operations where the weights are zeros. This also allows FAT to benefit from the  $16\times$  storage reduction without compressed sparse formats.

Second, we propose a fast addition scheme at the circuit level based on the memory Sense Amplifier. We store the intermediate carry in a latch and compute the summation of two operands in only one step. This avoids the time overhead of both waiting for the propagation of the carry and writing the carry back to the memory.

Third, we propose a Combined-Stationary data mapping scheme to make full use of the computational capacity of the proposed accelerator. The Image-to-Column based channel-distributed mapping reduces the data movement of activations, weights and output feature maps together for lower energy cost. Compared with direct mapping, the proposed mapping

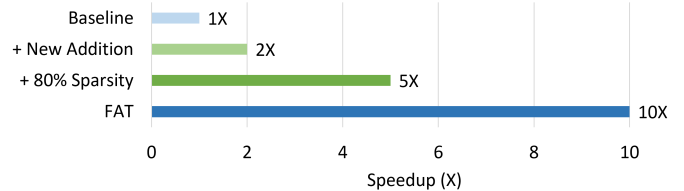


Fig. 1. The speedup breakdown of TWNs with 80% sparsity on our FAT.

can achieve near 100% column parallelism in memory arrays and  $18\times$  speedup.

Our proposed TWN accelerator FAT combines the speedup from fast addition and sparsity together, as Fig.1 shows. Taking the SOTA IMC BWN accelerator ParaPIM [32] as the baseline, the proposed fast addition scheme based on the Sense Amplifier provides  $2.00\times$  fast and  $1.22\times$  power-efficient addition operator. Our Sparse Addition Control Unit provides another  $5.00\times$  speedup with 80% layer sparsity. In total FAT is up to  $10.02\times$  faster and  $12.19\times$  energy-efficient than ParaPIM on quantized CNNs with 80% sparsity.

## II. RELATED WORKS AND MOTIVATION

### A. Non-Volatile Memory and In-Memory-Computing

Memory access is one of the main performance and energy bottlenecks in traditional computing systems. Because moving the data from memory to processing units for computation and sending back the result to the memory lead to long latency and huge power consumption. Thus placing the logic near or even inside the memory have been proposed to mitigate this problem, namely Near-Memory Computing (NMC) [37], [38] and In-Memory Computing (IMC) [22], [21]. NMC places the logic closer to the memory, while IMC utilizes the memory arrays to do computation.

IMC can be realized using Static Random-Access Memory (SRAM) [39], Dynamic RAM (DRAM) [40] and Non-Volatile Memories (NVMs) including Resistive RAM (ReRAM) [41], Ferroelectric RAM (FeRAM) [42], STT-MRAM [22], Spin-Orbit Torque MRAM (SOT-MRAM) [32] and other emerging memory devices [21]. NVMs outperform SRAM and DRAM with near-zero leakage power and the non-volatile property of the stored data [43], while STT-MRAM and SOT-MRAM outperform other NVMs with  $\sim 10^{15}$  write endurance of single memory cell and much shorter access latency [44]. Therefore, this paper chooses STT-MRAM as the basic memory cell.

The standard STT-MRAM memory cell contains one Magnetic-Tunnel-Junction (MTJ) and one access transistor connected to the Bit-Line (BL), the Word-Line (WL) and the Source-Line (SL) as Fig.2 (a) shows. The MTJ has a pinned layer as the reference and a free layer whose magnetic orientation direction can be switched by memory writes. A tunnelling oxide isolates the pinned layer and the free layer. The MTJ has a low resistance in the "parallel state" where the free layer has the same magnetic orientation direction as the pinned layer, and it has a high resistance in the other "anti-parallel state". Applying the same current to the STT-MRAM memory cell, the Sense Amplifier receives a voltage  $V_{sense}$  as

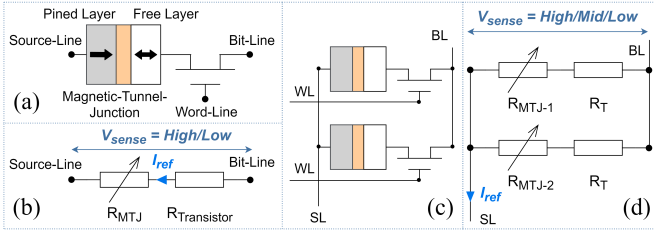


Fig. 2. The STT-MRAM memory cells and the abstracted circuit. (a) Standard 1T-1MTJ STT-MRAM memory cell. (b) The equivalent circuit of one activated memory cell. (c) Activating two rows of memory cells simultaneously. (d) The equivalent circuit of two activated memory cells.

shown in Fig.2 (b). The anti-parallel state MTJ gives a high sensed voltage (can be identified as "1") while the parallel state MTJ provides a low sensed voltage (identified as "0").

Similarly, In-Memory-Computing takes advantage of the resistance of the memory cells to do computation. For example, activating two rows of STT-MRAM memory cells simultaneously as Fig.2 (c) and (d) show, the sensed voltage can be high (the two cells storing "11"), middle (storing "01"/"10") or low (storing "00"). Thus the Sense Amplifier can perform computations like Boolean functions between the operands in the activated cells by identifying the sensed voltage, and this is the basic idea of In-Memory-Computing.

### B. In-Memory-Computing Accelerators for Quantized CNNs

We review the related works on IMC accelerators for quantized neural networks in Table II. As IMC architectures are able to compute Boolean functions and the addition operation, IMC based CNN accelerators mainly focus on ternary and binary networks: TNNs and BNNs, which quantize both the weights and activations to 2-bit/1-bit values and the main operations are Boolean operations, and TWNs and BWNs that only quantize the weights and the primary operation is addition. The accelerators can also be categorized into traditional memory based (SRAM and DRAM) and NVM based (ReRAM, FeRAM, STT-MRAM, SOT-MRAM, etc) according to the memory type.

BNNs replace the 1-bit multiplication with XNOR and the 1-bit accumulation with popcnt (count the number of "1"s in a binary value) in the binary dot product. So the BNN accelerators target XNOR and popcnt for high speedup. RRAM-BNN [41], XNOR-BNN [43] and PIMBALL [45] utilize the XOR/XNOR operations of the ReRAM, SRAM and STT-MRAM memory arrays to process the BNNs. Some related works build special memory cells to accelerate BNNs. For example, 2T2R-TCAM [46] creates a 2-transistor-2-ReRAM (2T2R) Ternary Content Addressable Memory (TCAM) which supports in-memory logic and XNOR/XOR based binary dot product. VR-XNOR [47] proposes a memristor-based Voltage-Resistance XNOR (VR-XNOR) cell with a filter bank for binary convolution acceleration. Some papers also use traditional memories, especially SRAM, as processing elements for BNNs. SRAM-CIM [39] raises an SRAM Computing-In-Memory (SRAM-CIM) unit-macro for binarized fully connected neural networks. XNOR-SRAM [28] presents an

TABLE II  
RELATED IMC ACCELERATORS ON BINARY AND TERNARY NETWORKS.

CNN	Target Ops	NVM Based	Tradi. Mem. Based
BNN	XNOR + Popcnt	RRAM-BNN [41] PIMBALL [45] XNOR-BNN [43] 2T2R-TCAM [46] VR-XNOR [47]	XNOR-SRAM [28] SRAM-CIM [39] XNOR-BNN [43]
TNN	Ternary Mul., or Gated-XNOR + Popcnt	4T2R-IM-DP [48] SpinLiM [49] TeC-Cell [50] Ter-LiM [52]	TiM-DNN [27] XNOR-SRAM [28] IMC-CD-TNN [51]
BWN	Dense Addition	ParaPIM [32] MRIMA [33]	
TWN	Sparse Addition	This Work	

SRAM macro that supports ternary-XNOR-and-accumulate operations for both BNNs and TNNs.

TNN acceleration is another active research area besides BNN acceleration. The dominant operation in TNNs is ternary multiplication which is equivalent to a Gated-XNOR followed by a popcnt, so most TNN accelerators build dedicated processing units for 2-bit ternary multiplications. 4T2R-IM-DP [48] provides a ReRAM-based IMC 4T2R bit-cell which enables In-Memory Dot Product (IM-DP) for TNNs. Ter-LiM [52] implements a Ternary Logic-in-Memory (Ter-LiM) scheme based on the memristive dual-crossbar structure with multi-level memristor cells. SpinLiM [49] utilizes two 2T-2MTJ SOT-MRAM cells to realize the ternary multiplication. TeC-Cell [50] proposes a Non-Volatile Ternary Compute-Enabled memory cell (TeC-Cell) based on ferroelectric transistors as well as TeC-Arrays to perform parallel signed ternary multiplications. The SRAM based TNN accelerators in related works also introduce special processing units for the ternary multiplications. For example, TiM-DNN [27] proposes Ternary-in-Memory (TiM) tiles for parallel signed ternary vector-matrix multiplications based on CMOS Ternary Processing Cells with memory and ternary multiplication functions. IMC-CD-TNN [51] realizes the ternary multiplication with switch-capacitor ternary neurons and the wide vector summation in charge domain to accelerate TNNs.

BWNs transform the multiplications into additions rather than the Boolean operations like BNNs and TNNs, so BWN accelerators utilize the addition and memory array level parallelism in IMC devices. ParaPIM [32] takes advantage of the parallel addition in SOT-MRAM memory arrays for efficient in-memory addition and convolution, while MRIMA [33] leverages the massive parallelism across the STT-MRAM memory banks, matrices and arrays to accelerate BWNs. As a result, ParaPIM and MRIMA both achieve higher performance and energy efficiency than DRAM based, ReRAM based and ASIC based accelerators.

TWNs are different from BWNs due to the 2-bit weights, the higher accuracy and the network sparsity. To the best of our knowledge, this work is the first sparse IMC accelerator for TWNs. This work builds more efficient addition operations than ParaPIM and MRIMA. This paper also takes the 2-bit representation and the network sparsity into account to enable

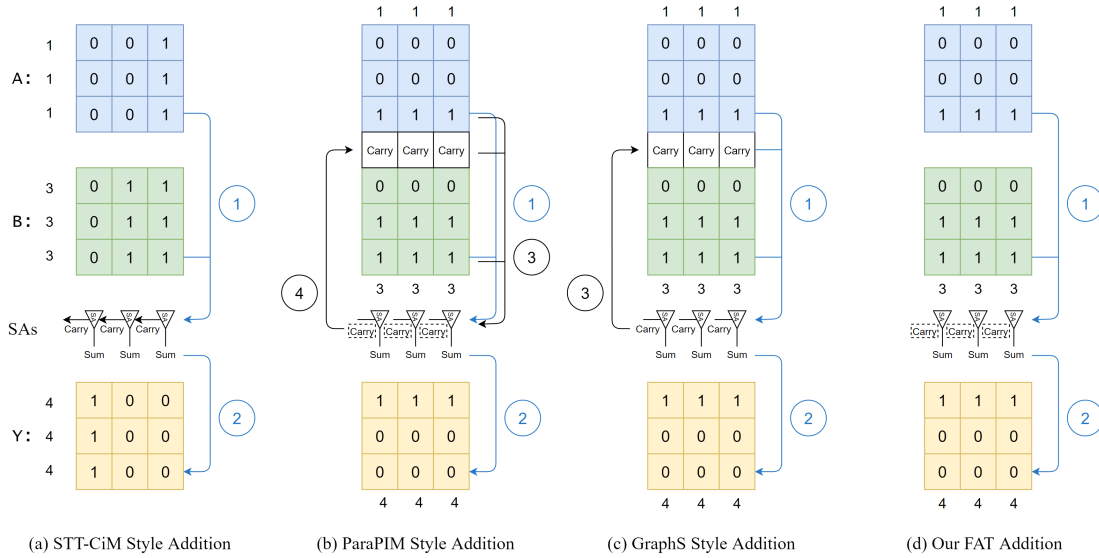


Fig. 3. Addition schemes in STT-CiM series [29], [30], [31], ParaPIM series [32], [33], GraphS series [34], [35], [36] IMC devices and our proposed FAT.

sparse additions for lower latency and higher energy efficiency.

### C. In-Memory-Computing Addition Schemes

Existing IMC devices are able to perform Boolean functions and Addition operations. The mainstream IMC addition schemes can be categorized into STT-CiM series, ParaPIM series and GraphS series as Fig. 3 shows. We will review and analyze the addition schemes in these related works and propose our efficient addition scheme in this subsection.

STT-CiM series devices [29], [30], [31] store the values in rows as Fig. 3 (a) shows. The upper two arrays stand for the operands  $A=(1, 1, 1)$  and  $B=(3, 3, 3)$ . First, the Sense Amplifier (SA) of STT-CiM reads two operands together and analyze the total current to calculate the summation result  $Y=A+B$ . Second, the SA outputs the addition result  $Y=(4, 4, 4)$ , and the result can be stored in the memory array at the bottom. This addition scheme is logically straightforward and efficient for scalar addition. But it also has two shortcomings: First, it needs to wait for the carry to propagate to the last bit, so the latency is long, and the latency increases linearly with the operand bitwidth. Second, the vector addition in  $N$  rows has  $N$  times latency as one scalar addition.

ParaPIM [32] and MRIMA [33] are IMC accelerators for BWNs based on SOT-MRAM and STT-MRAM respectively. ParaPIM series accelerators store the values in columns as Fig. 3 (b) shows. For example, operand 1 encoded as "001" is stored in a column rather than a row in the first memory array A. ParaPIM series accelerators perform the addition bit by bit rather than finish the scalar addition in one step. The advantage of this addition scheme is that it has the same latency for vector addition and scalar addition as long as the vector length doesn't exceed the number of memory columns. But it also has two weaknesses: First, it computes the Sum and Carry-out sequentially, which brings long latency. Second, this addition scheme needs to write the Carry-out back to the memory to

utilize it as the Carry-in for the next bit, which results in extra latency and energy cost.

GraphS [34], ParaPIM-SA-II [35] and CA-DNN-PIM [36] adopt a new SA design to overcome the first weakness of ParaPIM series addition while keeping a similar workflow. GraphS series devices compute the Sum and Carry-out in one step as Fig. 3 (c) shows and achieves  $1.3\times$  performance/area as ParaPIM. But GraphS series devices still have two problems: First, GraphS only has  $0.8\times$  energy-efficiency/area as ParaPIM due to its complex 3-operand logic and the increased area. Second, GraphS series accelerators still store back and read in the intermediate carry results to/from the memory array following ParaPIM, bringing unnecessary latency and power consumption.

To overcome the shortcomings of existing addition schemes, we propose an efficient addition scheme at the algorithm level along with a novel SA at the circuit level. Our FAT style fast addition operation does not need to wait for the propagation of the carry nor write the carry back to the memory as illustrated in Fig. 3 (d). First, similar to ParaPIM and GraphS, we store the operands in columns and compute the summation bit by bit. The bit by bit addition avoids the latency of waiting the propagation of the carry. Second, instead of storing the intermediate carry of the previous bit back to the memory array, we keep it into a D-latch inside the SA to make it more energy-efficient. Third, we compute the summation by reading in two operands in only one step with the Carry-in (same as the Carry-out from the previous bit) stored inside the SA, which brings a shorter critical path for addition operations. Also, we only need 2-operand logic functions instead of the 3-operand logic functions in ParaPIM and GraphS, reducing the power and increasing the sensing reliability.



### III. ACCELERATOR FAT

We present our accelerator FAT in this section, including the architecture overview, the IMC memory array, and the data mapping method. The memory array features two components: the Sparse Addition Control Unit (SACU), which provides a sparse vector dot product, and the Sense Amplifier (SA), which implements the proposed fast addition scheme. In addition, the Combined-Stationary data mapping method reduces the data movement and increases the parallelism of memory arrays.

#### A. Overview

Our accelerator, FAT, is an STT-MRAM based In-Memory-Computing (IMC) accelerator for Ternary Weight Neural Network (TWN) inference. FAT also supports Binary Weight Neural Network (BWN) inference with few configurations. We will explain the accelerated networks, the accelerator architecture and the basic workflow in this subsection.

1) *Target Applications*: The typical basic block of a CNN comprises a convolution or fully connected layer followed by an activation function and a batch normalization layer. The convolution and fully connected layers are computation-intensive, while the activation and batch normalization layers have much fewer floating-point operations than the other two layers. For example, convolution of activation  $X$  and weight  $W$  needs  $C \cdot KH \cdot KW$  multiplications for every output point as equation (1) shows, where  $KN$ ,  $C$ ,  $KH$ ,  $KW$  are the number of filters, channel, kernel height and kernel width. But the popular activation ReLU and the batch normalization are much simpler than convolution, as equations (2)-(3) show.

$$Y_{kn,h,w} = \sum_{c=1}^C \sum_{i=1}^{KH} \sum_{j=1}^{KW} X_{c,h+i,w+j} \cdot W_{kn,c,i,j} \quad (1)$$

$$\text{ReLU}(x) = \begin{cases} x, & x > 0 \\ 0, & x \leq 0 \end{cases} \quad (2)$$

$$\text{BN}(Y) = \frac{Y - E[Y]}{\sqrt{\text{Var}[Y] + \epsilon}} \quad (3)$$

The weights in TWNs are quantized to ternary values to reduce the computation complexity of convolution and fully connected layers. The weights are ternarized to  $\{+1, 0, -1\}$  by comparing with trained or given thresholds as equation (4) shows, where  $w$  and  $w^t$  are the original and ternarized weight values, and  $TH_{low}$  and  $TH_{high}$  are the thresholds. Modern TWNs train the weights to be ternary values [14], [15], [16], so the weights of target neural networks are already quantized into 2-bit numbers when the training finishes.

$$w^t = \begin{cases} +1, & w > TH_{high} \\ -1, & w < TH_{low} \\ 0, & otherwise \end{cases}, TH_{low} < TH_{high} \quad (4)$$

$$y = \vec{x} \cdot \vec{w}^t = \sum_{i=1}^N \vec{x}_i \cdot \vec{w}_i^t, \vec{w}^t \in \{\pm 1, 0\}^N \quad (5)$$

The convolution and matrix multiplication in convolution and fully connected layers can be decomposed as the inner dot

product between the activation vector  $\vec{x}$  and the weight vector  $\vec{w}^t$  as equation (5) shows, where  $N$  is the vector length. The ternarized weights in TWNs further simplify the dot product into addition/subtraction and null operations (multiplying zero is non-sense). Therefore, we build FAT to accelerate TWNs with two main features: the low-level fast addition and the high-level addition based sparse dot product which skips the null operations. FAT is also able to inference BWNs because the weights of BWNs only contain  $\{+1, -1\}$ , but BWN inference has no performance benefit from the sparsity.

2) *Accelerator Architecture*: Our accelerator FAT consists of Computing Memory Arrays (CMAs) and a CMOS Data Processing Unit (DPU) as Fig. 4 (a) shows. The CMAs are in charge of the addition operations in convolution and fully connected layers, so the CMAs are equipped with proposed SACU and SA for sparse dot product and efficient addition operation. The DPU takes care of the batch normalization and activation layers. We keep almost the same DPU architecture as ParaPIM [32] and MRIMA [33] except that our DPU has no hardware quantizer. As the weights of modern TWNs and BWNs are trained to be 2-bit ternary values or 1-bit binary values, which means the weights are already quantized before inference, so the weight quantizer is not necessary. Excluding the quantizer may reduce the chip area, power, and inference time thanks to no procedure on quantization. In summary, the CMAs with sparse dot product and efficient addition work together with the DPU containing activation functions and batch normalization to finish the TWN inference.

3) *Computation Workflow*: FAT conducts the inference block by block, and the workflow of one example convolution block is shown in Fig. 4 (b). First, the activations of each convolution layer are loaded to the memory cells of CMAs. Second, the weights of each layer are loaded to the Sparse Addition Control Unit inside the Memory Controller. The loading of weights may repeat many times as there are many filters in a convolution layer. Then the Memory Controller performs parallel computation across memory columns. All the CMAs with loaded activations and weights can process the convolution layer in parallel. Fourth, the convolution results are sent to the DPU through the internal buses. Fifth, the DPU performs the activation function and batch normalization to

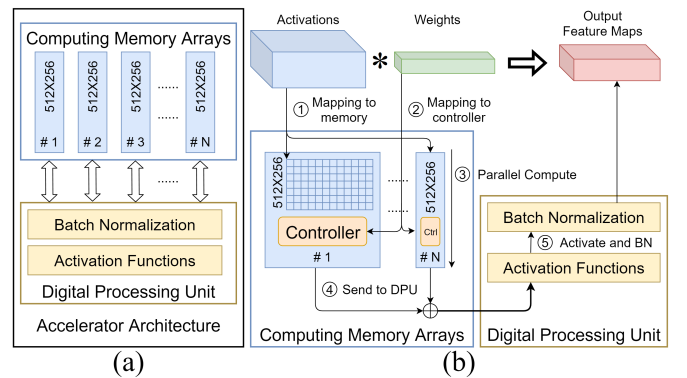


Fig. 4. (a) The architecture of FAT. (b) The computation workflow of FAT.

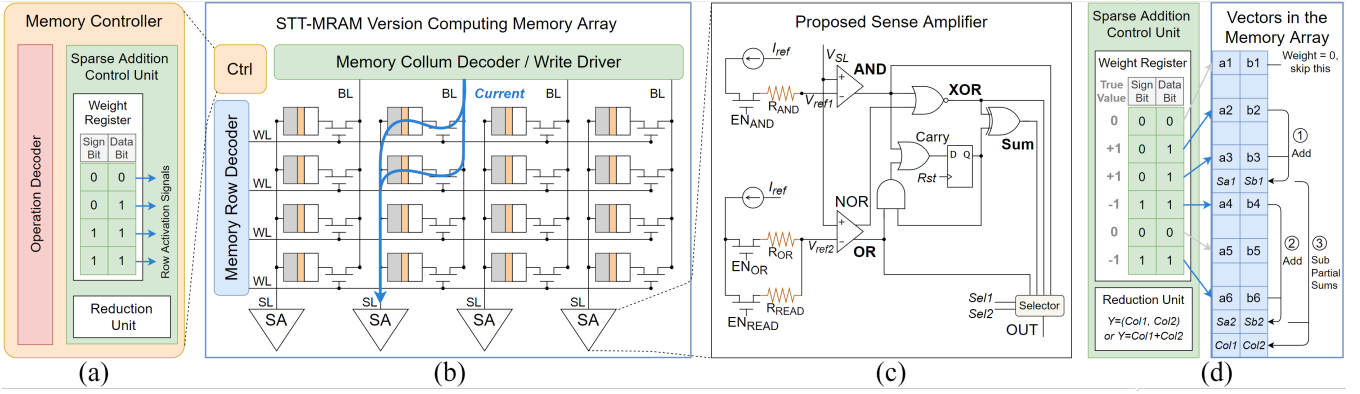


Fig. 5. Overview of FAT Computing Memory Array. (a) The architecture of the Memory Controller. (b) The architecture of the Computing Memory Array. (c) The architecture of the Sense Amplifier. (d) The workflow of addition based sparse dot product controlled by the Sparse Addition Control Unit.

generate the output feature maps. After all, the output feature maps are stored again to CMAs as activations for the next layer. We repeat this process until we get the output of the whole neural network.

### B. Computing Memory Array

The Computing Memory Array (CMA) consists of a Memory Controller (MC), a Memory Row Address Decoder (MRAD) which controls the Word-Lines (WLs), a Memory Column Address Decoder (MCAD)/Writer Driver that controls the Bit-Lines (BLs), a memory array, and Sense Amplifiers (SAs) connected to the Source-Lines (SLs) as Fig. 5 shows. Our CMA works in three modes: a standard memory device mode with basic Read/Write support, a general-purpose computation mode that enables the Boolean functions and the Addition function, and a TWN accelerator mode.

Working as a standard memory device or a general-purpose IMC device, the MC receives the signals from a CPU and sends control signals to other components to perform Read, Write, Boolean and Addition operations. The MRAD/MCAD decodes the row/column addresses based on the signals from MC and activates the WLs/BLs to access target memory cells. Then the SA receives the current from the memory array by the SL and produces the corresponding result of Read, Boolean functions or Addition.

Working as a TWN accelerator, our CMA provides two main features. First, the Sparse Addition Control Unit (SACU) inside the MC enables the high-level sparse vector dot product. Second, the SA facilitates the low-level fast Addition. We will introduce the SACU and the SA in the following two subsections in detail.

1) *Sparse Addition Control Unit*: When processing a convolution layer or a fully connected layer in TWNs, the weights determine which operands of the activations should be added together. Therefore, we store the activations inside the memory array to conduct addition operations. At the same time, we load the weights into the MC, or to be exact, the inside Sparse Addition Control Unit (SACU).

TABLE III  
UTILIZE THE WEIGHTS TO SKIP THE NULL OPERATIONS.

Weight	Sign Bit	Add/Sub	Data Bit/Mask	Activate this row?
+1 (01)	0	Add	1	Yes
0 (00)	0	Null	0	No
-1 (11)	1	Sub	1	Yes

a) *Architecture*: The architecture of the SACU is shown in Fig. 5 (a). It contains weight registers and a reduction unit. The SACU uses weight registers to generate the control signals of the sparse dot product. The reduction unit can accumulate the summations in different columns when necessary.

The weights of TWNs only have three values, namely  $\{+1, 0, -1\}$ . Thus we adopt the encoding of standard signed integer for the weights as Table III shows. The 2-bit encoding contains a sign bit and a data bit which can determine what operation should be applied to the activations in corresponding rows. The sign bit shows whether this is an addition (sign bit=0) or a subtraction (sign bit=1), but +1(01) and 0(00) share the same sign bit "0", so we need the data bit to work as a mask. Therefore, we activate the corresponding rows only when data bit=1 so that the rows corresponding to weight 0(00) have no operation. In other words, the null operations are skipped during the sparse dot product.

b) *Sparse Addition Workflow*: As mentioned in the previous paragraph, the data bit of the weight determines whether the operands in the corresponding row need operation and the sign bit indicates the operation type is addition or subtraction. This motivates us how to conduct the addition based sparse dot product, and the workflow is shown in Fig. 5 (d). The SACU generates the row activation signals based on the data in the weight register. Then the MRAD enables the corresponding rows of operands for addition. The addition based sparse dot product has three stages. First, we add those rows that need addition together and get a partial sum in each column. Second, we add those rows that need subtraction together and get another partial sum in every column. Third, we perform a subtraction operation (which is also supported in FAT) between these two partial sums to get the summation result of this column. This three-stage addition pipeline separates

the operands corresponding to weight +1 and -1. In this way, we can perform addition operations only on all the activation operands, and the partial sums only need one subtraction operation. As the subtraction in FAT has one more step than the addition, our three-stage addition pipeline is optimized to use fewer subtractions for less latency.

Taking Fig. 5 (d) with the weight vector being (0, +1, +1, -1, 0, -1) as an example, there are two vectors  $a$  and  $b$  in the memory array to perform dot product with the weights. First, we add the operands corresponding to weight +1, so the SACU activates row 2 and row 3 simultaneously to add them together, and the partial sums  $Sa1$  and  $Sb1$  are calculated at the same time. Second, we add the operands corresponding to weight -1, so the SACU adds row 4 and row 6 together, and the partial sums are  $Sa2$  and  $Sb2$ . Finally, we accumulate the partial sums to get the summation of the whole column, so the SACU performs  $Col1 = Sa1 - Sa2$  and  $Col2 = Sb1 - Sb2$  in parallel.

Our sparse dot product has two features: skipping the null operations where weights are zeros and having high column level parallelism. The SACU only activates the rows where the weights are +1 or -1, so our FAT automatically skips the addition operations corresponding to zero weights. As the example shows above, the memory columns can be activated simultaneously, so FAT has outstanding memory column level parallelism. This column level parallelism can boost the performance if combined with suitable data mapping and scheduling methods, which will be explored in the Data Mapping section.

We mentioned in the accelerator overview that FAT could also work as a BWN accelerator with simple configurations. We only need to extend the 1-bit binary weight data (+1 and -1) to 2-bit signed integer encoding as Table III shows, then store the 2-bit binary values into weight registers in the SACU, and FAT will work as a BWN accelerator. However, the SACU will activate all the rows based on the weights in this case, so there will be no benefit from sparsity.

2) *Sense Amplifier*: The Sense Amplifier (SA) is the core component of an In-Memory-Computing (IMC) device because it determines which kinds of operations the device support. Our motivation drives us to design an SA that supports faster and more efficient addition operations than related works. Furthermore, our SA is able to conduct common Boolean functions and subtraction not limited to the addition operation. We will introduce the SA architecture, the supported operations, and the comparison with related works in the following paragraphs.

a) *Architecture and Workflow*: Our SA's architecture is presented in Fig. 5 (c). The signal flow inside the SA has four stages: sensing, comparing, combining, and selecting. We will follow the signal flow to show how our SA works.

**Sensing**: In the sensing stage, the Word-Line (WL) and the Bit-Line (BL) are activated, and the current flows through the target memory cells to the Source-Line (SL) as Fig. 5 (b) shows. The equivalent circuit of the sensing state is illustrated in Fig. 6 (a). So the Operational Amplifier (OpAmp) in the

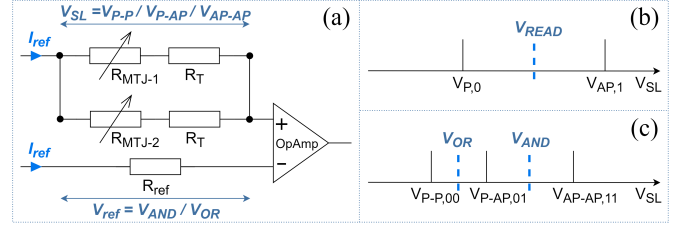


Fig. 6. (a) The equivalent circuit when sensing two memory cells at the same time. (b) The reference voltage  $V_{READ}$  of sensing one memory cell. (c) The reference voltages  $V_{AND}$  and  $V_{OR}$  of sensing two memory cells.

SA gets the total current from the SL along with the voltage of SL  $V_{SL}$  as equation (6) shows, where  $I_{ref}$  is the reference activation current, and  $R_{MTJ}$  and  $R_T$  are the resistances of the MTJ and the access transistor in a memory cell.

$$V_{SL} = I_{ref} \cdot ((R_{MTJ1} + R_{T1}) / (R_{MTJ2} + R_{T2})) \quad (6)$$

$$V_{ref} = I_{ref} \cdot R_{ref} \quad (7)$$

**Comparing**: Getting the sensed voltage  $V_{SL}$ , the OpAmp in the SA compares it with reference voltages to get the result of READ, AND or OR, which can be further used to compute more complex functions. The sensed voltage  $V_{SL}$  of reading out a single memory cell can be either a lower voltage  $V_{P,0}$  when the MTJ is in parallel state (storing a "0") or a higher voltage  $V_{AP,1}$  with an anti-parallel state MTJ (storing a "1"). So the reference voltage for reading  $V_{READ}$  lies between  $V_{P,0}$  and  $V_{AP,1}$  as Fig. 6 (b) shows. Similarly, the sensed voltage  $V_{SL}$  of reading out two memory cells can be  $V_{P-P,00}$ ,  $V_{P-AP,01}$  and  $V_{AP-AP,11}$  as Fig. 6 (c) shows. So the reference voltage of AND  $V_{AND}$  lies between  $V_{P-AP,01}$  and  $V_{AP-AP,11}$ , while the  $V_{OR}$  is between  $V_{P-P,00}$  and  $V_{P-AP,01}$ .

$$A \text{ XOR } B = [\underline{A \text{ AND } B}] \text{ NOR } [\underline{A \text{ NOR } B}] \quad (8)$$

$$SUM = [\underline{A \text{ XOR } B}] \text{ XOR } Cin \quad (9)$$

$$Cout = ([\underline{A \text{ OR } B}] \text{ OR } Cin) \text{ AND } [\underline{A \text{ AND } B}] \quad (10)$$

**Combining**: Next, the other logic gates in the SA combine the AND, OR and NOR signals generated by the OpAmps to compute more complex functions, e.g., XOR, SUM and Carry-out of the Addition operation as presented in Fig. 5 (c). For example, the XOR is calculated by NOR between the AND and NOR of operand A and B as equation (8) shows, where the underlined parts in the square brackets are signals generated by the OpAmp from the comparing stage. Similarly, the SUM and the Carry-out  $Cout$  are calculated following equation (9)-(10) where  $Cin$  is the Carry-in from the previous bit stored in the D-Latch. Thus, our SA uses four logic gates (NOR, XOR, OR and AND) and one D-Latch in the combining stage as presented in equation (8)-(10) and Fig. 5 (c).

**Selecting**: Finally, the selector selects the desired result based on the selecting signals Sel1 and Sel2, and sends it to the output port OUT.

b) *Configuration and Supported Operations*: Our SA can perform READ, NOT, AND, NAND, OR, XOR, and Addition (ADD) functions natively and Subtraction (SUB) extensively.

So it relies on the enable signals and selector signals from the Memory Controller (MC) to give the desired result. We configure the enable signals of the SA to perform different functions according to Table IV. Meanwhile, we select the results routed to the input ports of the selector as Table V shows, then we get the desired result at the OUT port.

The SA supports eight functions but building eight selector ports for all the functions brings high complexity and large area cost. So we optimize the SA on the functionality of READ, NOT, NAND and SUB, and simplify the design to only four selector ports. First, the READ and OR operations share the same OR selector port because they use the same OpAmp. Second, as the NOT equals to XOR with "1"s as equation (11) shows, we read in the operand along with a row filled with "1"s and produce the NOT result at the XOR selector port. RISC-V has adopted the same technique to simplify the instruction set by replacing NOT with XOR [53]. Third, we disable the enable signals of EN\_OR and EN\_READ at the second OpAmp in the SA when computing the NAND. The NOR port of the OpAmp will be "0"s for any  $V_{SL}$  higher than zero. Then the NAND result appears at the XOR port after a NOR between the AND and "0"s, as equation (12) shows. Last, as the SUB equals to ADD the opposite number as shown in equation (13), we perform the SUB operation by one NOT followed by one ADD with the first carry-in to be "1".

$$\text{NOT } A = A \text{ XOR } 111\dots1 \quad (11)$$

$$A \text{ NAND } B = (A \text{ AND } B) \text{ NOR } 000\dots0 \quad (12)$$

$$A - B = A + ((\text{NOT } B) + 1) \quad (13)$$

Therefore, our SA has the least number of enabling (EN) signals, selector signals and amplifiers among related works as inferred from Table VI. But the fast addition operation enabled by our SA costs one D-latch and four Boolean gates. The area of the SAs can also be inferred from Table VI. The SA of STT-CiM will have less area than ours due to one less D-latch, but STT-CiM has four more control signals than FAT. The SA of FAT will have a smaller area than ParaPIM's SA because we have fewer control signals and a smaller output selector. Operational amplifiers usually have a much larger area than Boolean gates due to higher complexity and higher loading capacity. The SA of FAT will be smaller than GraphS'

TABLE IV  
CONFIGURATION OF ENABLE SIGNALS OF THE SENSE AMPLIFIER.

Operation	READ	NOT	AND	NAND	OR	XOR	ADD
EN_RD	1	0	0	0	0	0	0
EN_AND	0	1	1	1	0	1	1
EN_OR	0	1	0	0	1	1	1
Sel. Port	OR	XOR	AND	XOR	OR	XOR	SUM

TABLE V  
CONFIGURATION OF SELECTOR SIGNALS OF THE SENSE AMPLIFIER.

Selector Port	AND	OR	XOR	SUM
Sel 1	0	0	1	1
Sel 2	0	1	0	1

TABLE VI  
COMPARISON OF PROPOSED SA AND SAs IN RELATED WORKS.

Name	Signals		Circuits		
	EN	Selector	Amplifier	D-Latch	Boolean Gates
STT-CiM	6	3	2	0	4
ParaPIM	4	3	2	1	3
GraphS	6	3	3	0	1
Our FAT	3	2	2	1	4

SA, which has one more operational amplifier and a larger selector. The exact area and speed comparison will be given in the Evaluation section.

*c) Fast Addition:* We propose the new SA to adopt the efficient addition scheme shown in Fig. 3 (d). Temporarily our CMA works as a sequential 1-bit adder and computes the summation bit by bit to realize the N-bit addition. First, the MC initializes the D-Latch containing the Carry in the SA as 0 before the addition operation. Next, the MCAD enables those columns containing the operands, and the MRAD activates two rows catering to two bits of the operands simultaneously. The reference current flows through the memory cells to the SA. Then the SA computes the summation (SUM) of these two bits and stores the carry-out of the current bit in the Carry Latch to use it as the carry-in of the next bit. This unique design avoids storing back the carry-out results to the memory and saves a considerable amount of energy compared with ParaPIM [35] and GraphS series IMC accelerators. The bit-by-bit addition also prevents the latency of carry propagation which exists in the STT-CiM series devices. So the proposed addition operation is referenced as fast addition. The additions in IMC devices are all addition between integers or fixed-point numbers. So the activations also need to be stored in fixed-point numbers rather than floating-point numbers.

Our fast addition operation is throughput driven rather than latency driven. FAT has shorter addition latency than ParaPIM and GraphS because we don't need to store back the carries to the memory cells. But FAT has longer latency than STT-CiM series IMC devices in single scalar addition because we compute the summation bit by bit. FAT's advantage lies in the vector addition, where hundreds to thousands of pairs of operands need addition results. Thanks to the column-wise data storage format shown in Fig. 3, the bit-by-bit addition in FAT, ParaPIM and GraphS has N times parallelism as the scalar addition in STT-CiM series devices in N-bit vector addition. Supposing the addition operands are two  $1024 \times 32$ -bit vectors, they are stored in 1024 columns and 32 rows inside a memory array with 1024 columns and 512 rows. FAT repeats the 1-bit addition 32 times to get the vector addition result because the operand vector is stored in 1024 columns vertically. But STT-CiM needs to perform the 32-bit addition 32 times across the memory array because the operand vector is stored in 32 rows horizontally. FAT conducts the 1-bit additions while STT-CiM repeats the 32-bit additions, so our FAT has less latency than STT-CiM in vector additions.

In summary, our FAT style vector addition is faster than STT-CiM, ParaPIM, and GraphS. The Evaluation section will provide a detailed performance comparison of these works.



```

0 # The Output-Stationary (OS) style direct convolution algorithm
1 for n in range(N):
2     for kn in range(KN):
3         for oh in range(OH):
4             for ow in range(OW):
5                 for c in range(C):
6                     for kh in range(KH):
7                         for kw in range(KW):
8                             y[n][kn][oh][ow] += w[kn][c][kh][kw]
9                             * x[n][c][oh*s+kh][ow*s+kw]
0 # The Combined-Stationary (CS) style Img2Col/GEMM based conv of FAT
1 for kn in range(KN):
2     # Combine kn with i or j with duplicated activations if possible
3     for n in range(N):
4         # Combine n with i to map to the memory columns if possible
5         for i in range(OH*OW):
6             # Map i to the memory columns, wholly parallel
7             for j in range(C*KH*KW):
8                 # Map j to the memory rows, sequential addition
9                 Ay[n][kn][i] += Aw[kn][j] * Ax[n][i][j]

```

Fig. 7. The Output-Stationary direct convolution algorithm and the Combined-Stationary Img2Col/GEMM based convolution algorithm.

### C. Data Mapping

FAT is a TWN accelerator with faster addition operation at the circuit level and utilizes the TWN sparsity at the architecture level. We further explore the data mapping schemes to optimize the memory utilization, performance and energy cost. We will take the convolution layer as an example to present our mapping scheme

1) *Existing Convolution and Mapping Methods*: We usually perform convolution in direct convolution or Img2Col/GEMM based convolution. The weights slide across the activations and perform vector dot product in direct convolution, which is presented in the first algorithm of Fig. 7. For an activation tensor in shape  $[N, C, H, W]$  (Batch Size, Channel, Height, Width) and the weight tensor in shape  $[KN, C, KH, KW]$  (Number of Filters, Channel, Kernel Height, Kernel Width), the shape of output feature map tensor is  $[N, KN, OH, OW]$  (Batch Size, Output Channel, Output Height, Output Width). Direct convolution is straightforward to implement. Its implementations can reduce memory usage due to the data reuse in the sliding windows. However, the standard direct convolution involves stride  $S$ , which may decrease the data reuse. Furthermore, direct convolution is a sequential algorithm, it is not efficient for achieving high parallelism.

Therefore, Img2Col/GEMM based convolution is introduced to reduce the data dependency and improve the parallelism. Image-to-Column (Img2Col) transforms the activations into 2D arrays as Fig. 8 (a) shows, taking the convolution stride into account. Then a General Matrix Multiplication (GEMM) between the unrolled weights and the transformed activations computes the convolution results. Img2Col only keeps the activations needed for convolution, so the data-level parallelism can be maximized without being affected by the convolution stride.

The upper convolution algorithm needs to be mapped to the hardware for execution. There are four main ways of mapping the convolution data to accelerators, namely Weight-Stationary (WS), Input-Stationary (IS), Output-Stationary (OS) and Row-Stationary (RS) [18], [54], [55]. WS is optimized to reuse

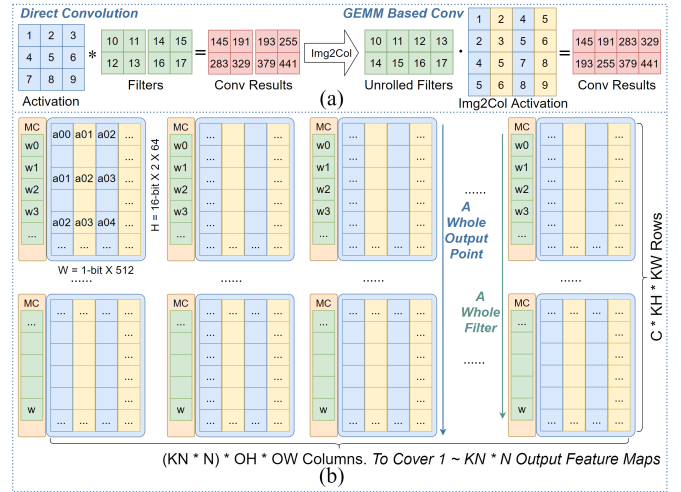


Fig. 8. (a) Img2Col transforms convolution into GEMM. (b) Illustration of our Combined-Stationary mapping scheme.

the weights and reduce the movement of weights. Similarly, IS and OS are optimized to reuse the activations and the (intermediate) convolution results, respectively. Fig. 7 provides an example of OS mapping in direct convolution. We can infer from the algorithm that the OS style mapping tries to keep the output feature map tensor  $y$  in the inner loop unchanged as long as possible. While RS aims to optimize the memory access of DRAMs as accessing the DRAM data in consecutive rows has less latency and energy.

The mentioned convolution and mapping methods are optimized for on-the-shelf platforms like GPU and other traditional deep learning accelerators rather than IMC accelerators. Though some mapping methods for IMC platforms have been proposed [56], their target memory arrays are different from ours because they load the weights to the memory crossbars for computation. In contrast, we load the weights to the memory controllers to control the sparse addition. The following paragraphs will select and modify the existing mapping methods to fit the proposed IMC accelerator FAT's features.

2) *Img2Col Based Combined-Stationary Mapping*: Several factors affect the selection of convolution and mapping methods on our IMC accelerator for TWNs. First, the memory arrays are throughput driven with high parallelism across columns. So Img2Col based convolution is more favoured than direct convolution on IMC devices because it decouples the sliding window convolution into a parallel GEMM problem. Second, the weights of TWNs are now quantized into 2-bit numbers, but the activations are still 16-bit/32-bit fixed-point numbers. So reusing the weights may not bring as many benefits as reusing the activation. Third, the weights are loaded into SRAM based weight registers inside the SACUs, while the activations are loaded into STT-MRAM based memory arrays. The STT-MRAM memory cells have limited endurance of writes rather than the unlimited lifespan of SRAM, so keeping the activations in the memory arrays rather than moving them is essential.

Therefore, we select the Img2Col/GEMM based convolution

TABLE VII  
COMPARISON OF MAPPING METHODS IN CONVOLUTION LAYERS.

Mapping	X Loads	W Loads	Parallel Columns	Occupied Memory Arrays	Execution Time
Direct-OS	$N*KN*KH$	$N*KH*KW$	$\min(MW/S, W/S)$	$[C/MH]*H*[W/MW]$	$N*KH*KW*(MH+[C/MH])$
Img2Col-OS	$N*KN*KH*KW$	$N*KH*KW$	$\min(MW, OH*OW)$	$[C/MH]*[OH*OW/MW]$	$N*KH*KW*(MH+[C/MH])$
Img2Col-WS	$N*KN$	1	$\min(MW, OH*OW)$	$[C/MH]*KH*KW*[OH*OW/MW]$	$N*(MH+KH*KW*[C/MH])$
Img2Col-IS	N	$N*KH*KW$	$\min(MW/(KH*KW), OH*OW)$	$[C/MH]*[KH*KW*OH*OW/MW]$	$N*KH*KW*(MH+[C/MH])$
Img2Col-CS	1	1	$\min(MW, N*OH*OW)$	$[C*KH*KW/MH]*[N*OH*OW/MW]$	$MH+[KH*KW*C/MH]$
I2C-CS-Itvl.	1	1	$\min(MW, N*OH*OW)$	$[2*C*KH*KW/MH]*[N*OH*OW/MW]$	$MH/2+[2*KH*KW*C/MH]$

TABLE VIII  
COMPARISON OF MAPPING METHODS IN AN EXAMPLE CONVOLUTION LAYER (LAYER 10 OF RESNET-18).

Mapping	Load Times		Para. Cols Real/Max	Primary Mapping		Scaled-up Mapping						Endur.
	X	W		CMA	Runtime	CMA	Utiliz.	X Writes	W Writes	Runtime	Speedup	
Direct-OS	3840	11520	14/256	1x28=28	1486080	28	5.5%	385.4M	10569.6M	1486080	1.0	128
Img2Col-OS	11520	11520	196/512	1x1=1	1486080	36	38.3%	10404.5M	13589.5M	41280	36.0	128
Img2Col-WS	1280	256	196/512	9x1=9	175360	36	38.3%	1156.1M	0.3M	43840	33.9	128
Img2Col-IS	5	11520	56/56	1x4=4	1486080	36	86.1%	10.2M	5.9M	165120	9.0	128
Img2Col-CS	1	256	512/512	9x2=18	35072	36	95.7%	1.1M	1.5M	17536	84.7	128
I2C-CS-Itvl.	1	256	512/512	18x2=36	20992	36	47.9%	1.1M	1.5M	20992	70.8	1

with Input-Stationary (IS) mapping scheme as the base mapping method for our IMC accelerator FAT. The Img2Col convolution can bring high data-level parallelism using GEMM. We further propose two optimizations upon the base mapping. First, we distribute the channel of the Img2Col activation across memory arrays to utilize the column parallelism in our CMAs fully. The channel number is usually multiples of 64 and can occupy several columns in the memory array, e.g., M columns. But the weights loaded to each memory array only correspond to one column, and we can only parallel process the first column in every M columns. So we need to distribute the channel across memory banks to ensure that one channel only occupies one column in one memory array. Then we can process all the columns in parallel. Second, we store the activation in the memory arrays with intervals whose height equals one operand. The IS mapping keeps the activations in the memory arrays for as long as possible to reduce the write times of STT-MRAM memory cells. Still, the accumulation of immediate results also needs many write operations to the memory cells. Therefore, we store the activation in the memory arrays with intervals to leave room for immediate results. Now the immediate addition results are stored in these operand intervals rather than in a fixed place. As a result, the memory writes are distributed to half of all the memory cells, and the memory cells lifetime will be more balanced.

We name our mapping as Combined-Stationary (CS) style mapping as shown in Fig. 7 and Fig. 8 (b). The  $A_x$ ,  $A_w$  and  $A_y$  in the second algorithm of Fig. 7 refer to the activation array, the weight array and the output feature map array after Img2Col. The height and the width of the output feature maps are combined as one dimension, with the length being  $OH*OW$ . And the new dimension  $OH*OW$  is mapped to the memory columns horizontally for parallel processing. The channel, the height and the width of the filter are combined as one dimension whose length is  $C*KH*KW$ . The new dimension  $C*KH*KW$  is mapped to the memory rows vertically for

sequential addition. As mentioned in the second optimization in the previous paragraph, we distribute  $C*KH*KW$  across memory arrays to compute one output feature map point in only one aligned column among memory arrays. The weights are loaded to the SACU to control the sparse addition, which takes place across all the memory columns in the whole memory array as Fig. 8 (b) shows.

The basic CS style mapping can be scaled up if there is available space. The first choice is scaling up across the activations. We can load in more activation arrays and duplicate the weights for higher parallelism across the batch size N. The second scaling up option is across the weights. We can duplicate the activation arrays and load more filters for higher parallelism across filters KN.

3) *Mapping Method Analysis*: We compare the mapping methods in Table VII and Table VIII. The compared mapping methods include the OS style mapping in direct convolution (Direct-OS), the OS, WS, and IS style mapping in Img2Col/GEMM based convolution (Img2Col-OS/WS/IS), our proposed CS style mapping (Img2Col-CS), and CS style mapping with intervals (I2C-CS-Itvl).

Table VII shows the loading times of activation tensor X and filter tensor W in the first two columns. The numbers have been simplified to show the relative ratios only. Img2Col-WS reduces the data loading on weights, and Img2Col-IS reduces the data loading on activations compared with Img2Col-OS, which correspond to their features. Our Img2Col-CS and I2C-CS-Itvl combine the WS and IS to reduce the loading of activations and weights together. Img2Col-CS and I2C-CS-Itvl also increase the upper bound of parallel columns by N times, where N is the batch size. The MW and MH stand for the memory width and height, e.g., how many operands can be stored in one memory column. The S stands for the convolution stride. As mentioned in the review of existing mapping methods, Img2Col based convolution can improve the parallelism by dealing with the stride in the Img2Col

transformation. The execution time in Table VII corresponds to the number of occupied memory arrays without considering the scaling-up, so the execution time of these mapping methods may be equal to each other. Approximately our CS style mapping is  $2*N*KH*KW$  times faster than the Direct-OS. Thus *Img2Col-CS* and *I2C-CS-Itvl* can achieve  $18\times$  speedup than the baseline when the batch size is one in convolution layers with  $3\times 3$  kernels.

We take layer 10 of ResNet-18 as an example convolution layer to give a showcase of the actual performance of these mapping methods in Table VIII, where  $(N, C, H, W)=(5, 128, 28, 28)$ ,  $(KN, C, KH, KW)=(256, 128, 3, 3)$  and stride  $S=2$ . Supposing the memory array has 512 columns, and each column can contain 128 operands, where  $(MW, MH)=(512, 128)$ . We first conduct a primary mapping of these methods, then scale them up to use the same number of CMAs for fair comparison because more CMAs provide higher performance.

First, our CS style mapping achieves the maximum 512-column parallelism inside the CMAs with a total of 512 columns. In contrast, the OS, WS and IS style mapping are bounded by the output size  $OW*OH$  or the parallelism capacity. Second, when scaled up to use 36 memory arrays, our *Img2Col-CS* achieves the highest memory utilization (95.7%) with the most negligible data loading of activations and weights. The  $>200\times$  less memory write on both the activations and the weights compared with *Direct-OS* and *Img2Col-OS* shows that our CS mapping is very energy-efficient. Third, the performance gains of *Img2Col-OS* and *Img2Col-WS* are remarkable. Even so, *Img2Col-CS* and *I2C-CS-Itvl* outperform them by about  $2\times$ . Fourth, *I2C-CS-Itvl* improves the write balance by  $128\times$  at a slight performance cost. One STT-MRAM cell has limited  $\sim 10^{15}$  writes in a lifetime. *I2C-CS-Itvl* leaves intervals at the memory rows to reduce the write times of the cells storing immediate addition results. As a result, *I2C-CS-Itvl* achieves  $128\times$  (or up to  $MH\times$  in ordinary cases) fewer writes on the immediate result cells. It significantly increases the lifetime of the CMAs at the cost of half memory utilization as *Img2Col-CS* and only 16.4% performance drop. So *I2C-CS-Itvl* is the most efficient mapping method for our accelerator FAT.

#### IV. EVALUATION

We implement the Sense Amplifiers (SAs) of FAT and related works using NCSU 45nm FreePDK45™ library [57], [58]. We adopt the comparator of STT-CiM [29] and include the output selector for all the four SAs for a fair comparison. We build, verify and evaluate the circuits in Cadence Virtuoso IC6.1.8 using Virtuoso ADEL, Spectre and Layout Suite XL to obtain the corresponding latency, power and area. We refer to [59] for the write time of 1-Transistor-1-Junction STT-MRAM memory array implemented in the same 45nm process.

The performance gain of our accelerator comes from the improvements in the addition operation and the sparsity. The first subsection evaluates the SAs on the performance and efficiency of IMC operations. Then we evaluate the network level performance with sparsity in the second subsection.

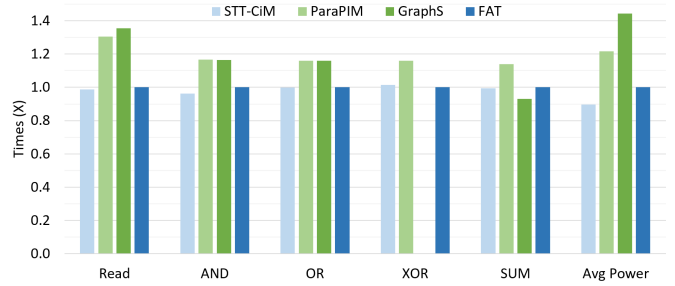


Fig. 9. Normalized critical path latency and dynamic power of IMC operations in Sense Amplifiers of FAT and relate works.

#### A. Sense Amplifier Level Performance

1) *Latency and Power of In-Memory-Computing Operations*: We first compare the performance of IMC operations in different SAs, including STT-CiM, ParaPIM, GraphS and our proposed FAT. Fig.9 presents the normalized dynamic power and normalized latency of the Read, AND, OR, XOR, and SUM operations. The SA latency calculates from receiving the sensing signal coming from the memory cells to getting the operation output at the OUT port. STT-CiM [29] has slightly lower latency than FAT in Read ( $<1.3\%$ ), AND ( $<3.7\%$ ), OR ( $<0.2\%$ ) and SUM ( $<0.7\%$ ) due to its simple SA architecture. But STT-CiM has 1.4% higher latency than FAT in XOR operation because our FAT has fewer loading devices at the XOR result port. Also, our FAT has four fewer configuration signals than STT-CiM.

Our FAT outperforms ParaPIM [32] about 30% on Read,  $>15\%$  on AND, OR and XOR and 14% on SUM. Our reusable output port design only needs a 4-to-1 selector rather than an 8-to-1 selector, which contributes to less latency of FAT. Our FAT is 35% faster than GraphS [34] on Read, and  $>15\%$  faster on AND and OR. GraphS is 7% faster than FAT on SUM thanks to its aggressive computation scheme, but it does not support XOR. Our FAT is also  $1.22\times$  and  $1.44\times$  more power-efficient than ParaPIM and GraphS respectively.

2) *Latency and Efficiency of Addition Operation*: We present the simulation results of the Critical Path (CP) in the SA and the latency of addition operations in Table IX. We include the time of writing back the result to the memory array in the latency of 8-bit scalar addition and the 8-bit /16-bit vector addition. The addition schemes of STT-CiM, ParaPIM, GraphS and our proposed FAT are different. STT-CiM computes the 8-bit addition in one step as mentioned in Fig. 3, but the other three methods need to perform the 8-bit addition in 8 steps. So STT-CiM has the shortest critical

TABLE IX  
THE CRITICAL-PATH (CP) AND LATENCY OF ADDITION OPERATIONS IN FAT AND RELATED WORKS.

Type	Scalar ADD		Vector ADD			
	8-bit		8-bit		16-bit	
Bitwidth	CP	Latency	CP	Latency	CP	Latency
STT-CiM	<b>0.41</b>	<b>8.91</b>	3.26	71.26	10.85	146.85
ParaPIM	2.47	138.47	2.47	138.47	4.95	276.95
GraphS	1.18	137.18	1.18	137.18	2.36	274.36
FAT	<b>1.13</b>	<b>69.13</b>	<b>1.13</b>	<b>69.13</b>	<b>2.26</b>	<b>138.26</b>

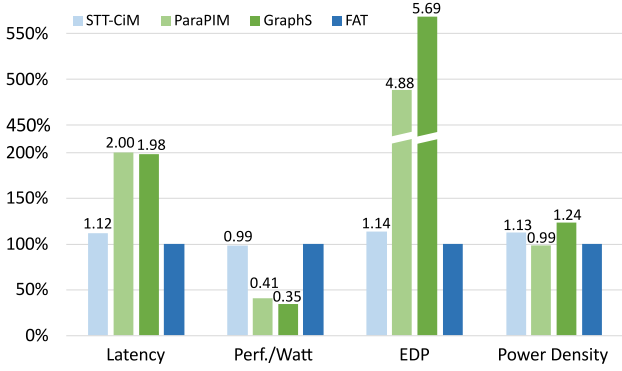


Fig. 10. Normalized latency and efficiency of 32-bit Addition of FAT and related works.

path and shortest latency when performing one scalar addition operation. The ParaPIM series, GraphS series, and proposed FAT style addition conduct the addition bit by bit. One 8-bit addition and adding two 8-bit vectors have the same eight steps in the bit-by-bit style addition, as long as the vector length does not exceed the memory array width. So adding two scalars and adding two vectors share the same latency in these three methods. Our FAT outperforms ParaPIM and GraphS in the critical path, single addition and vector addition thanks to the new SA and the proposed efficient addition scheme that stores the carry in the latch instead of the memory array. FAT also has shorter latency than STT-CiM on vector addition because STT-CiM has to repeat the addition for N times in the N-bit vector addition.

Our FAT builds the SA for the most efficient vector addition among related works. As neural networks are throughput-driven and TWNs utilize vector additions in convolution layers, vector addition is more important than single scalar addition in TWN accelerators. We take the 32-bit vector addition to analyze further the performance and efficiency of these SAs in Fig. 10, including the latency, performance/watt, Energy-Delay-Product (EDP), and power density (power/area).

First, FAT is 1.12 $\times$ , 2.00 $\times$  and 1.98 $\times$  faster than STT-CiM, ParaPIM and GraphS respectively in 32-bit vector addition. Taking the write overhead of the SUM and Carry into account, we find that ParaPIM and GraphS are much slower than STT-CiM due to the extra write of Carry. Though GraphS has less computation latency in the SA, the write of Carry to the memory is so time-consuming that it slows down the whole vector addition operation. Our FAT has a shorter critical path in the SUM and avoids the propagation of Carry in STT-CiM, so we have the shortest computation latency. We also avoid the extra write of Carry in ParaPIM and GraphS, so we have the shortest vector addition latency.

Second, FAT has the highest performance/watt and is 1.01-2.86 $\times$  efficient than related works. Third, our FAT has the least EDP among related works and is 1.14-5.69 $\times$  efficient than STT-CiM, ParaPIM and GraphS. Fourth, FAT has a lower power density than STT-CiM and GraphS, which means our FAT is more balanced on the power distribution and may have a longer lifetime.

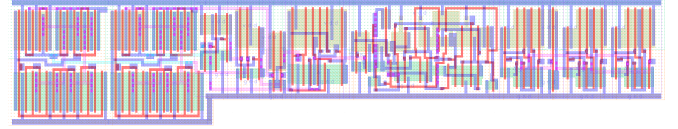


Fig. 11. Layout of our Sense Amplifier in Virtuoso Layout Suite XL.

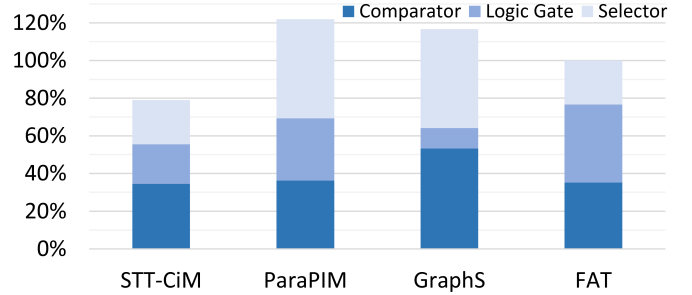


Fig. 12. Area breakdown of the Sense Amplifiers in FAT and related works.

In summary, we realize a vector addition with high performance and high efficiency for TWNs by innovation from the addition scheme and the SA circuit.

3) *Area and Reliability of Sense Amplifiers*: We present the layout of our SA in Fig.11 for reference. The area of our proposed FAT and related works are shown in Fig.12. We normalize the area to FAT for easy comparison. FAT has 21% more area than STT-CiM because of the D-Latch, but it is 1.22 $\times$  and 1.17 $\times$  area efficient than ParaPIM and GraphS, respectively. ParaPIM has seven output ports, so it needs an 8-input multiplexer and has a larger size than STT-CiM. GraphS has fewer logic gates than ParaPIM, but it uses three comparators, so it has a similar area as ParaPIM. Our FAT has more logic gates than other SAs, but FAT uses only two comparators and a 4-input selector, so it has less area cost than ParaPIM and GraphS.

Also, our SA is more reliable than ParaPIM and GraphS. FAT's SA only contains two-operand operations rather than three-operand operations like ParaPIM and GraphS. The sense margin of two-operand operations is 2.4 $\times$  as high as that of three-operand operations [32], [33], [34], [35]. As a larger sense margin brings less error rate, our SA is more reliable than ParaPIM and GraphS.

### B. Network Level Performance

We take ParaPIM as the baseline to present the network level performance and the energy efficiency in Fig. 13 because only ParaPIM series devices are BWN IMC accelerators among the three series related works. The overall performance improvement is determined by both the fast addition and the sparsity. We achieve 2.00 $\times$  speedup and 1.22 $\times$  power efficiency compared with ParaPIM from the novel addition scheme with the new SA. The SACU further brings speedups from the sparsity of the TWNs. Our accelerator can achieve 3.34 $\times$  network level speedup and 4.06 $\times$  energy efficiency when the sparsity is 40%, 5.01 $\times$  speedup and 6.09 $\times$  energy efficiency with 60% sparsity, and 10.02 $\times$  speedup and 12.19 $\times$  energy efficiency with 80% sparsity.



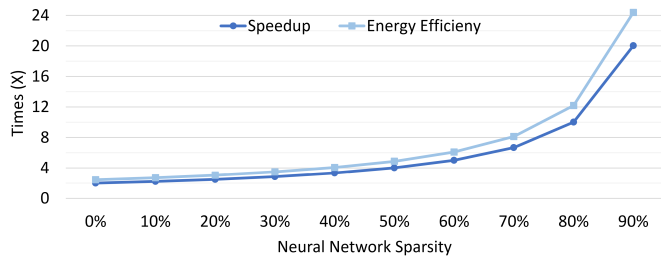


Fig. 13. Speedup and energy efficiency of neural networks across sparsity.

## V. CONCLUSION

In this paper, we propose FAT as an In-Memory-Computing accelerator with fast addition and sparse dot product for Ternary Weight Neural Networks. We propose an efficient in-memory addition scheme and a new Sense Amplifier that stores the carry inside the Sense Amplifier to avoid the carry propagation latency and carry writing back latency. Our Sense Amplifier is  $2.00\times$  faster,  $1.22\times$  power-efficient and  $1.22\times$  area efficient than ParaPIM and MRIMA on addition operations. We propose a Sparse Addition Control Unit which utilizes the sparsity of TWNs to skip the addition operations corresponding to zero weights. FAT with the sparse dot product achieves up to  $10.02\times$  speedup and  $12.19\times$  energy efficiency on networks with 80% sparsity compared with ParaPIM and MRIMA. We further present the Combined-Stationary mapping to reach near 100% column parallelism across the whole memory array, which brings about  $18\times$  speedup to convolution layers with  $3\times 3$  kernels compared with direct mapping.

## ACKNOWLEDGMENT

This work is partially supported by the Ministry of Education, Singapore, under its Academic Research Fund Tier 2 (MOE2019-T2-1-071) and Tier 1 (MOE2019-T1-001-072), and partially supported by Nanyang Technological University, Singapore, under its NAP (M4082282) and SUG (M4082087).

## REFERENCES

- [1] M. Tan and Q. Le, "Efficientnet: Rethinking model scaling for convolutional neural networks," in *International Conference on Machine Learning*. PMLR, 2019, pp. 6105–6114.
- [2] M. Tan, R. Pang, and Q. V. Le, "Efficientdet: Scalable and efficient object detection," in *Proceedings of the IEEE/CVF conference on computer vision and pattern recognition*, 2020, pp. 10781–10790.
- [3] A. Baevski, Y. Zhou, A. Mohamed, and M. Auli, "wav2vec 2.0: A framework for self-supervised learning of speech representations," *Advances in Neural Information Processing Systems*, vol. 33, 2020.
- [4] X. Liu, K. Duh, L. Liu, and J. Gao, "Very deep transformers for neural machine translation," *arXiv preprint arXiv:2008.07772*, 2020.
- [5] M. Savva, A. Kadian, O. Maksymets, Y. Zhao, E. Wijmans, B. Jain, J. Straub, J. Liu, V. Koltun, J. Malik, D. Parikh, and D. Batra, "Habitat: A Platform for Embodied AI Research," in *Proceedings of the IEEE/CVF International Conference on Computer Vision (ICCV)*, 2019.
- [6] E. Wijmans, A. Kadian, A. Morcos, S. Lee, I. Essa, D. Parikh, M. Savva, and D. Batra, "DD-PPO: Learning near-perfect pointgoal navigators from 2.5 billion frames," in *International Conference on Learning Representations, ICLR*, 2020.
- [7] M. Rastegari, V. Ordonez, J. Redmon, and A. Farhadi, "Xnor-net: Imagenet classification using binary convolutional neural networks," in *European conference on computer vision*. Springer, 2016, pp. 525–542.
- [8] Z. Cai, X. He, J. Sun, and N. Vasconcelos, "Deep learning with low precision by half-wave gaussian quantization," in *Proceedings of the IEEE conference on computer vision and pattern recognition*, 2017, pp. 5918–5926.
- [9] H. Pouransari, Z. Tu, and O. Tuzel, "Least squares binary quantization of neural networks," in *Proceedings of the IEEE/CVF Conference on Computer Vision and Pattern Recognition Workshops*, 2020, pp. 698–699.
- [10] F. Zhu, R. Gong, F. Yu, X. Liu, Y. Wang, Z. Li, X. Yang, and J. Yan, "Towards unified int8 training for convolutional neural network," in *Proceedings of the IEEE/CVF Conference on Computer Vision and Pattern Recognition*, 2020, pp. 1969–1979.
- [11] K. Zhao, S. Huang, P. Pan, Y. Li, Y. Zhang, Z. Gu, and Y. Xu, "Distribution adaptive int8 quantization for training cnns," in *Proceedings of the AAAI Conference on Artificial Intelligence*, 2021.
- [12] R. Li, Y. Wang, F. Liang, H. Qin, J. Yan, and R. Fan, "Fully quantized network for object detection," in *Proceedings of the IEEE/CVF Conference on Computer Vision and Pattern Recognition*, 2019, pp. 2810–2819.
- [13] X. Sun, N. Wang, C.-Y. Chen, J. Ni, A. Agrawal, X. Cui, S. Venkataramani, K. El Maghraoui, V. V. Srinivasan, and K. Gopalakrishnan, "Ultra-low precision 4-bit training of deep neural networks," *Advances in Neural Information Processing Systems*, vol. 33, 2020.
- [14] C. Zhu, S. Han, H. Mao, and W. J. Dally, "Trained ternary quantization," in *5th International Conference on Learning Representations, ICLR*. OpenReview.net, 2017.
- [15] Y. Li, X. Dong, S. Q. Zhang, H. Bai, Y. Chen, and W. Wang, "Rtn: Reparameterized ternary network," in *Proceedings of the AAAI Conference on Artificial Intelligence*, vol. 34, no. 04, 2020, pp. 4780–4787.
- [16] Y. Li, W. Ding, C. Liu, B. Zhang, and G. Guo, "Trq: Ternary neural networks with residual quantization," in *Proceedings of the AAAI Conference on Artificial Intelligence*, 2021.
- [17] A. Parashar, M. Rhu, A. Mukkara, A. Puglielli, R. Venkatesan, B. Khailany, J. Emer, S. W. Keckler, and W. J. Dally, "SCNN: An accelerator for compressed-sparse convolutional neural networks," *ACM SIGARCH Computer Architecture News*, vol. 45, no. 2, pp. 27–40, 2017.
- [18] Y.-H. Chen, T.-J. Yang, J. Emer, and V. Sze, "Eyeriss v2: A flexible accelerator for emerging deep neural networks on mobile devices," *IEEE Journal on Emerging and Selected Topics in Circuits and Systems*, vol. 9, no. 2, pp. 292–308, 2019.
- [19] J. Choquette and W. Gandhi, "Nvidia a100 gpu: Performance amp; innovation for gpu computing," in *2020 IEEE Hot Chips 32 Symposium (HCS)*, 2020, pp. 1–43.
- [20] K. He, X. Zhang, S. Ren, and J. Sun, "Deep residual learning for image recognition," in *Proceedings of the IEEE conference on computer vision and pattern recognition*, 2016, pp. 770–778.
- [21] A. Sebastian, M. Le Gallo, R. Khaddam-Aljameh, and E. Eleftheriou, "Memory devices and applications for in-memory computing," *Nature nanotechnology*, vol. 15, no. 7, pp. 529–544, 2020.
- [22] S. Jain, S. Sapatnekar, J.-P. Wang, K. Roy, and A. Raghunathan, "Computing-in-memory with spintronics," in *2018 Design, Automation & Test in Europe Conference & Exhibition (DATE)*. IEEE, 2018, pp. 1640–1645.
- [23] C.-J. Jhang, C.-X. Xue, J.-M. Hung, F.-C. Chang, and M.-F. Chang, "Challenges and trends of sram-based computing-in-memory for ai edge devices," *IEEE Transactions on Circuits and Systems I: Regular Papers*, vol. 68, no. 5, pp. 1773–1786, 2021.
- [24] Y. Ma, Y. Du, L. Du, J. Lin, and Z. Wang, "In-memory computing: The next-generation ai computing paradigm," in *Proceedings of the 2020 on Great Lakes Symposium on VLSI*, 2020, pp. 265–270.
- [25] D. Fujiki, N. Chatterjee, D. Lee, and M. O'Connor, "Near-memory data transformation for efficient sparse matrix multi-vector multiplication," in *Proceedings of the International Conference for High Performance Computing, Networking, Storage and Analysis*, 2019, pp. 1–17.
- [26] A. Mehrabi, D. Lee, N. Chatterjee, D. J. Sorin, B. C. Lee, and M. O'Connor, "Learning sparse matrix row permutations for efficient spmm on gpu architectures," in *2021 IEEE International Symposium on Performance Analysis of Systems and Software (ISPASS)*. IEEE, 2021, pp. 48–58.
- [27] S. Jain, S. K. Gupta, and A. Raghunathan, "Tim-dnn: Ternary in-memory accelerator for deep neural networks," *IEEE Transactions on Very Large Scale Integration (VLSI) Systems*, vol. 28, no. 7, pp. 1567–1577, 2020.

- [28] S. Yin, Z. Jiang, J.-S. Seo, and M. Seok, "Xnor-sram: In-memory computing sram macro for binary/ternary deep neural networks," *IEEE Journal of Solid-State Circuits*, vol. 55, no. 6, pp. 1733–1743, 2020.
- [29] S. Jain, A. Ranjan, K. Roy, and A. Raghunathan, "Computing in memory with spin-transfer torque magnetic ram," *IEEE Transactions on Very Large Scale Integration (VLSI) Systems*, vol. 26, no. 3, pp. 470–483, 2017.
- [30] S. K. Thirumala, S. Jain, A. Raghunathan, and S. K. Gupta, "Non-volatile memory utilizing reconfigurable ferroelectric transistors to enable differential read and energy-efficient in-memory computation," in *2019 IEEE/ACM International Symposium on Low Power Electronics and Design (ISLPED)*. IEEE, 2019, pp. 1–6.
- [31] S. K. Thirumala, Y.-T. Hung, S. Jain, A. Raha, N. Thakuria, V. Raghunathan, A. Raghunathan, Z. Chen, and S. Gupta, "Valley-coupled-spintronic non-volatile memories with compute-in-memory support," *IEEE Transactions on Nanotechnology*, vol. 19, pp. 635–647, 2020.
- [32] S. Angizi, Z. He, and D. Fan, "ParaPIM: A parallel processing-in-memory accelerator for binary-weight deep neural networks," in *Proceedings of the 24th Asia and South Pacific Design Automation Conference*, 2019, pp. 127–132.
- [33] S. Angizi, Z. He, A. Awad, and D. Fan, "Mrima: An mram-based in-memory accelerator," *IEEE Transactions on Computer-Aided Design of Integrated Circuits and Systems*, vol. 39, no. 5, pp. 1123–1136, 2019.
- [34] S. Angizi, J. Sun, W. Zhang, and D. Fan, "Graphs: A graph processing accelerator leveraging sot-mram," in *2019 Design, Automation & Test in Europe Conference & Exhibition (DATE)*. IEEE, 2019, pp. 378–383.
- [35] S. Angizi and D. Fan, "Deep neural network acceleration in non-volatile memory: A digital approach," in *2019 IEEE/ACM International Symposium on Nanoscale Architectures (NANOARCH)*. IEEE, 2019, pp. 1–6.
- [36] L. Yang, S. Angizi, and D. Fan, "A flexible processing-in-memory accelerator for dynamic channel-adaptive deep neural networks," in *2020 25th Asia and South Pacific Design Automation Conference (ASP-DAC)*. IEEE, 2020, pp. 313–318.
- [37] G. Singh, L. Chelini, S. Corda, A. J. Awan, S. Stuijk, R. Jordans, H. Corporaal, and A.-J. Boonstra, "A review of near-memory computing architectures: Opportunities and challenges," in *2018 21st Euromicro Conference on Digital System Design (DSD)*. IEEE, 2018, pp. 608–617.
- [38] —, "Near-memory computing: Past, present, and future," *Microprocessors and Microsystems*, vol. 71, p. 102868, 2019.
- [39] X. Si, W.-S. Khwa, J.-J. Chen, J.-F. Li, X. Sun, R. Liu, S. Yu, H. Yamauchi, Q. Li, and M.-F. Chang, "A dual-split 6t sram-based computing-in-memory unit-macro with fully parallel product-sum operation for binarized dnn edge processors," *IEEE Transactions on Circuits and Systems I: Regular Papers*, vol. 66, no. 11, pp. 4172–4185, 2019.
- [40] M. F. Ali, A. Jaiswal, and K. Roy, "In-memory low-cost bit-serial addition using commodity dram technology," *IEEE Transactions on Circuits and Systems I: Regular Papers*, vol. 67, no. 1, pp. 155–165, 2019.
- [41] X. Sun, X. Peng, P.-Y. Chen, R. Liu, J.-s. Seo, and S. Yu, "Fully parallel rram synaptic array for implementing binary neural network with (+ 1, -1) weights and (+ 1, 0) neurons," in *2018 23rd Asia and South Pacific Design Automation Conference (ASP-DAC)*. IEEE, 2018, pp. 574–579.
- [42] J. Wang, F. Wang, Z. Wang, W. Huang, Y. Yao, Y. Wang, J. Yang, N. Li, L. Yin, R. Cheng *et al.*, "Logic and in-memory computing achieved in a single ferroelectric semiconductor transistor," *Science Bulletin*, 2021.
- [43] X. Sun, R. Liu, X. Peng, and S. Yu, "Computing-in-memory with sram and rram for binary neural networks," in *2018 14th IEEE International Conference on Solid-State and Integrated Circuit Technology (ICSICT)*. IEEE, 2018, pp. 1–4.
- [44] S. H. Kang, "Embedded stt-mram for mobile applications: enabling advanced chip architectures," in *Non-volatile Memories Workshop*, 2010.
- [45] S. Resch, S. K. Khatamifard, Z. I. Chowdhury, M. Zabihi, Z. Zhao, J.-P. Wang, S. S. Sapatnekar, and U. R. Karpuzcu, "Pimball: Binary neural networks in spintronic memory," *ACM Transactions on Architecture and Code Optimization (TACO)*, vol. 16, no. 4, pp. 1–26, 2019.
- [46] Y. Chen, L. Lu, B. Kim, and T. T.-H. Kim, "Reconfigurable 2t2r reram with split word-lines for tcam operation and in-memory computing," in *2020 IEEE International Symposium on Circuits and Systems (ISCAS)*, 2020, pp. 1–5.
- [47] Y. Halawani, B. Mohammad, M. Abu Lebdeh, M. Al-Qutayri, and S. F. Al-Sarawi, "Reram-based in-memory computing for search engine and neural network applications," *IEEE Journal on Emerging and Selected Topics in Circuits and Systems*, vol. 9, no. 2, pp. 388–397, 2019.
- [48] Y. Chen, L. Lu, B. Kim, and T. T.-H. Kim, "A reconfigurable 4t2r reram computing in-memory macro for efficient edge applications," *IEEE Open Journal of Circuits and Systems*, vol. 2, pp. 210–222, 2021.
- [49] L. Luo, H. Zhang, J. Bai, Y. Zhang, W. Kang, and W. Zhao, "Spinlim: Spin orbit torque memory for ternary neural networks based on the logic-in-memory architecture," in *2021 Design, Automation and Test in Europe Conference and Exhibition (DATE)*, 2021, pp. 1865–1870.
- [50] S. K. Thirumala, S. Jain, S. K. Gupta, and A. Raghunathan, "Ternary compute-enabled memory using ferroelectric transistors for accelerating deep neural networks," in *2020 Design, Automation Test in Europe Conference Exhibition (DATE)*, 2020, pp. 31–36.
- [51] X. Yang, K. Zhu, X. Tang, M. Wang, M. Zhan, N. Lu, J. P. Kulkarni, D. Z. Pan, Y. Liu, and N. Sun, "An in-memory-computing charge-domain ternary cnn classifier," in *2021 IEEE Custom Integrated Circuits Conference (CICC)*. IEEE, 2021, pp. 1–2.
- [52] W. Liu, Y. Sun, W. He, and Q. Wang, "Design of ternary logic-in-memory based on memristive dual-crossbars," in *2021 IEEE International Symposium on Circuits and Systems (ISCAS)*, 2021, pp. 1–5.
- [53] RISC-V International. (2019) RISC-V Instruction Set Manual Volume I: User-Level ISA. [Online]. Available: <https://github.com/riscv/riscv-isa-manual/releases/download/Ratified-IMAFDQC/riscv-spec-20191213.pdf>
- [54] Y.-H. Chen, J. Emer, and V. Sze, "Eyeriss: A spatial architecture for energy-efficient dataflow for convolutional neural networks," *ACM SIGARCH Computer Architecture News*, vol. 44, no. 3, pp. 367–379, 2016.
- [55] H. Kwon, P. Chatarasi, M. Pellauer, A. Parashar, V. Sarkar, and T. Krishna, "Understanding reuse, performance, and hardware cost of dnn dataflow: A data-centric approach," in *Proceedings of the 52nd Annual IEEE/ACM International Symposium on Microarchitecture*, 2019, pp. 754–768.
- [56] X. Peng, R. Liu, and S. Yu, "Optimizing weight mapping and data flow for convolutional neural networks on rram based processing-in-memory architecture," in *2019 IEEE International Symposium on Circuits and Systems (ISCAS)*. IEEE, 2019, pp. 1–5.
- [57] North Carolina State University. (2011) NCSU FreePDK45. [Online]. Available: <https://research.ece.ncsu.edu/eda/freepdk/freepdk45/>
- [58] J. E. Stine, J. Chen, I. Castellanos, G. Sundararajan, M. Qayam, P. Kumar, J. Remington, and S. Sohoni, "Freepdk v2.0: Transitioning vlsi education towards nanometer variation-aware designs," in *2009 IEEE International Conference on Microelectronic Systems Education*. IEEE, 2009, pp. 100–103.
- [59] L. K. Vemula, N. M. Hossain, and M. H. Chowdhury, "Emerging stt-mram circuit and architecture co-design in 45nm technology," in *2017 IEEE 60th International Midwest Symposium on Circuits and Systems (MWSCAS)*. IEEE, 2017, pp. 719–722.